Differential Lipid Partitioning Between Adipocytes and Tissue Macrophages Modulates Macrophage Lipotoxicity and M2/M1 Polarization in Obese Mice

Xavier Prieur,[1] Crystal Y.L. Mok,[1] Vidya R. Velagapudi,[2] Vanessa Núñez,[3] Lucía Fuentes,[3] David Montaner,[4] Ko Ishikawa,[1] Alberto Camacho,[1] Nuria Barbarroja,[1] Stephen O'Rahilly,[1] Jaswinder K. Sethi,[1] Joaquin Dopazo,[4] Matej Orešič,[2] Mercedes Ricote,[3] and Antonio Vidal-Puig[1]

OBJECTIVE—Obesity-associated insulin resistance is characterized by a state of chronic, low-grade inflammation that is associated with the accumulation of M1 proinflammatory macrophages in adipose tissue. Although different evidence explains the mechanisms linking the expansion of adipose tissue and adipose tissue macrophage (ATM) polarization, in the current study we investigated the concept of lipid-induced toxicity as the pathogenic link that could explain the trigger of this response.

RESEARCH DESIGN AND METHODS—We addressed this question using isolated ATMs and adipocytes from genetic and diet-induced murine models of obesity. Through transcriptomic and lipidomic analysis, we created a model integrating transcript and lipid species networks simultaneously occurring in adipocytes and ATMs and their reversibility by thiazolidinedione treatment.

RESULTS—We show that polarization of ATMs is associated with lipid accumulation and the consequent formation of foam cell–like cells in adipose tissue. Our study reveals that early stages of adipose tissue expansion are characterized by M2-polarized ATMs and that progressive lipid accumulation within ATMs heralds the M1 polarization, a macrophage phenotype associated with severe obesity and insulin resistance. Furthermore, rosiglitazone treatment, which promotes redistribution of lipids toward adipocytes and extends the M2 ATM polarization state, prevents the lipid alterations associated with M1 ATM polarization.

CONCLUSIONS—Our data indicate that the M1 ATM polarization in obesity might be a macrophage-specific manifestation of a more general lipotoxic pathogenic mechanism. This indicates that strategies to optimize fat deposition and repartitioning toward adipocytes might improve insulin sensitivity by preventing ATM lipotoxicity and M1 polarization. ***Diabetes*** **60:797–809, 2011**

From the [1]Institute of Metabolic Science, Metabolic Research Laboratories, and Department of Clinical Biochemistry, University of Cambridge, Addenbrooke's Hospital, Cambridge, U.K.; the [2]Technical Research Centre of Finland (VTT), Espoo, Finland; the [3]Department of Regenerative Cardiology, Centro Nacional de Investigaciones Cardiovasculares, Melchor Fernández Almagro, Madrid, Spain; and the [4]Department of Bioinformatics and Genomics, Centro de Investigación Príncipe Felipe (CIFP), Functional Genomics Node (INB) at CIPF, Valencia, Spain.

Corresponding authors: Antonio Vidal-Puig, ajv22@cam.ac.uk, and Mercedes Ricote, mricote@cnic.es.

Received 17 May 2010 and accepted 14 December 2010.

DOI: 10.2337/db10-0705

This article contains Supplementary Data online at http://diabetes.diabetesjournals.org/lookup/suppl/doi:10.2337/db10-0705/-/DC1.

C.Y.L.M., V.R.V., and V.N. contributed equally to this article.

X.P. is currently affiliated with the Institut National de la Santé et de la Recherche Médicale U915, Institut du Thorax, Nantes, France.

Obesity-associated insulin resistance is characterized by a state of low-grade inflammation (1) that affects adipocyte function (2) and is associated with macrophage infiltration of adipose tissue (3). Additional evidence exists that diet-induced obesity (DIO) is associated with a switch in polarization of adipose tissue macrophages (ATMs) from an anti-inflammatory (M2) to a proinflammatory (M1) state (4,5). The pathogenic relevance of this change in polarization is highlighted by the specific clustering of M1 macrophages around necrotic crown-like structures, in contrast with the randomly scattered distribution of the anti-inflammatory M2 macrophages within adipose tissue (6). Diphtheria toxin–induced death of CD11c+ cells reduces crown-like structure formation and improves insulin sensitivity (7), subsequently emphasizing the pathogenic contribution of CD11c+ M1 macrophages to the metabolic syndrome.

To explain the primary propolarizing events, we recently proposed the adipose tissue expandability hypothesis (8,9), in which the link between obesity, inflammation, and metabolic complications is directly related to the failure of adipose tissue to expand and meet storage demands (10). We proposed that the impaired ability of adipose tissue to expand further and adipose dysfunction result in lipid spillage from adipocytes, thus promoting lipid toxicity and subsequent inflammation (11–13). Although indirect evidence indicates that dysregulated lipid metabolism may alter macrophage activation (13), the mechanism through which lipids exert their metabolic effects in these cells and which specific lipid species are involved remains unclear. On the basis of the expandability hypothesis (14), we speculated that obesity-induced polarization of ATMs may be another lipotoxic manifestation of the metabolic syndrome resulting from the ectopic accumulation of lipids in ATMs.

In this study, we investigated lipid-induced toxicity as the pathogenic link between expansion of adipose tissue and ATM polarization. Specifically, we studied ATMs and adipocytes in parallel from both genetic and diet-induced murine models of obesity at different stages of the development of obesity and insulin resistance. Our results indicate that M1 polarization is associated with the accumulation of lipid species and the proliferation of lipid droplets in ATMs, which then resemble vascular foam cells. The accumulation of lipids in ATMs coincided with the induction of gene-expression networks associated with lipid uptake, storage, and metabolism. Our research also reveals qualitative changes in the lipid species that accumulate in ATMs. Finally, we provide pharmacological

evidence that improving fat deposition in adipocytes promotes changes in the partitioning of lipids toward adipocytes and away from macrophages, which could prevent the proinflammatory switch of ATMs in severely obese mice.

RESEARCH DESIGN AND METHODS

Animals and biochemistry. Animals were housed in a temperature-controlled room (22°C) with a 12-h light/dark cycle. Food and water were available ad libitum. All animal protocols used in this study were approved by the U.K. Home Office. C57BL6 wild-type and *ob/ob* mice were purchased from Harlan (Oxon, U.K.) and placed on either a high-fat diet (45% calories from fat; D12451, Research Diets, New Brunswick, NJ) or a standard diet (RM3, with 11.5% of calories from fat; SDS, Essex, U.K.) with or without 10 ppm rosiglitazone (Avandia) for the time indicated in Fig. 7.

Adipose tissue fractionation. Gonadal or subcutaneous inguinal depots were removed after the mice were killed and then chopped thoroughly and resuspended in 10 mL digestion solution (7 mL Hanks' solution, 3 mL 7.5% BSA, and 20 mg collagenase type II; Sigma). The digestion was performed at 37°C using a shaker at 100 rpm for 20 min. After digestion, the adipocyte fraction (floating) was isolated and the solution containing the stroma vascular fraction was centrifuged at 1,500 rpm at 4°C for 5 min. The stroma vascular fraction pellet was resuspended in 1 mL selection buffer (PBS, 2 mmol/L EDTA, and 0.5% BSA), and the CD11b-positive cells were selected using CD11b microbeads (Miltenyi Biotec), according to the manufacturer's instructions.

Microarray. A total of 100 ng RNA ($n = 4$ per group) were biotin labeled using the Affymetrix GeneChip whole-transcript sense target–labeling assay (Affymetrix, High Wycombe, U.K.) and hybridized to Affymetrix mouse gene ST1.0 arrays. Affymetrix Power Tools (15) were used to perform microarray data normalization and preprocessing. CEL intensities where transformed using robust multi-array average (16) and quantile normalization (17). Differential gene expression was carried out using the limma (18) package from Bioconductor (http://bioconductor.org/). Gene-set analysis was carried out using logistic regression methods (19,20), as implemented in Babelomics (http://babelomics.org/) (21).

Flow cytometry. Fixed ATMs were incubated with BD Fc Block (BD Biosciences) for 5 min, followed by incubation with Bodipy 493/503 (Invitrogen) and/or specific monoclonal antibodies (GR1-Alexa 647, F4/80-PE-Cy7, and CD209a-APCp, eBioscience; CD11b-PE, BD Bioscience; Ly6C-Alexa 488 and CD206-Alexa-fluor 647, Serotec; and CD11c-PE, Miltenyi Biotec). After washing, ATMs were analyzed using FACSCalibur equipped with CellQuest Pro software (BD Biosciences). Nonspecific antibodies conjugated to the corresponding fluorochromes were used as negative controls, and the fluorescence threshold was set in order to have <5% of total cells positive for fluorescence. The percentage of positive cells (on a fixed number of events counted) for the antibodies of interest was determined by the percentage of cells exceeding the threshold obtained with nonspecific antibodies.

Lipidomic analysis. Adipocytes (5–10 mg) or ATMs (1.5–3.5 millions of cells) were diluted with 200 μL of 0.9% NaCl (for adipocytes samples) or 50 μL PBS buffer (for ATMs) and homogenized. The samples were subsequently extracted and analyzed using liquid chromatography–mass spectrometry as previously described (22).

Cell culture. Bone-marrow cells were isolated from C57BL6 males, differentiated for 7 days (RPMI supplemented with 30% of L-cells, 10% FBS, and 1% penicillin and streptomycin) and plated. Cells were treated with palmitate (500 μmol/L), palmitoleate (500 μmol/L), 0.4% endolipide (B-Braun Medical, Boulogne, France), or vehicle (ethanol) in 0.68% fatty acid–free BSA RPMI for 18 h.

Statistical analysis. All data were reported as means ± SE. All datasets were analyzed for statistical significance using the Student t test (Microsoft Excel). *$P < 0.05$; ** $P < 0.01$; *** $P < 0.001$.

RESULTS

Gene profiling of ATMs revealed biphasic expression of genes associated with M2 and M1 markers, extracellular matrix components, and lipid metabolism. We first studied ATM polarization in mice in two states: *1*) early, relatively mild stages of obesity in mice with relatively well-controlled glycemia despite insulin resistance; and *2*) in severely obese mice associated with insulin resistance and glucose intolerance. We compared ATMs from 5- and 16-week-old genetically obese *ob/ob* mice and wild-type lean controls (Supplementary Fig. 1*A*–*C*). These changes were consistent with time-dependent alterations in circulating adiponectin levels (Supplementary Fig. 1*D*).

An Affymetrix microarray platform was used to compare the gene-expression profiles of ATMs isolated from fresh gonadal white adipose tissue of *ob/ob* mice at 5 and 16 weeks of age and their respective wild-type controls (Fig. 1). ATMs were isolated by CD11b-MACS selection; purity was checked by flow cytometry. As shown in Supplementary Fig. 2*C*, 87% of the cells were positive for F4/80 and were therefore defined as ATMs. No granulocyte contamination was detected using the GR1 granulocyte marker (Supplementary Fig. 2).

Gene ontology (GO) (19) and the *Kyoto Encyclopedia of Genes and Genomes* (23) pathway analysis identified biphasic transcriptional profiles for genes associated with tissue pathways related to tissue repair/wound healing/extracellular matrix synthesis and with cell migration/adhesion/contraction (Fig. 1*A*). These pathways were induced at 5 weeks in *ob/ob* compared with wild-type mice (log odds ratio [LOR] >0). Conversely, they were repressed in *ob/ob* mice relative to wild-type mice at 16 weeks (LOR <0). Analysis of individual gene expression represented as heat maps support the same biphasic profile for genes involved in contraction (Fig. 1*B*) and extracellular matrix/remodeling (Fig. 1*C*). The high level of expression of genes involved in extracellular matrix/remodeling is a classical feature of M2 anti-inflammatory macrophages (Fig. 1*D*). At 5 weeks, ATMs from *ob/ob* mice showed increased expression of M2 anti-inflammatory macrophage markers (*ARG1* and *CD209e*) compared with wild-type controls, whereas the same M2 markers were repressed in ATMs from 16-week-old *ob/ob* mice. In contrast, at 16 weeks, there was increased expression of proinflammatory M1 markers (monocyte chemoattractant protein 1 [*MCP1*], tumor necrosis factor [*TNF*]α, interferon [*INF*] *INF*β, and *INF*$\alpha/\beta R$) in *ob/ob* ATMs. Altogether, these data indicate that in mild obesity, ATMs express a more M2-polarized profile associated with remodeling functions, whereas in severe obesity the expression of M2 markers decrease when M1-marker expression is induced. Interestingly, the only pathway repressed at 5 weeks and activated at 16 weeks, according to GO analysis, was the positive regulation of innate immune response (Fig. 1*A*).

In addition, several pathways involved in lipid metabolism were differentially regulated in *ob/ob* ATMs compared with wild-type ATMs. Expression of several genes involved in lipid uptake, handling, and accumulation (fatty acid transporter protein 1 [*FATP1*], *CD36*, adipose differentiation–related protein [*ADRP*], and lipoprotein lipase [*LPL*]) were upregulated in the ATMs of both 5- and 16-week-old *ob/ob* mice but not in wild-type controls (Fig. 1*E*).

An anti-inflammatory M2 profile in ATMs characterizes mild obesity and conserved glucose tolerance. We confirmed that at 5 weeks of age, arginase 1 [*ARG1*] and *CD209e* expression was higher in ATMs from *ob/ob* mice compared with wild-type mice. Conversely, at 16 weeks of age, *ARG1* and *CD209e* expression was lower in *ob/ob* versus wild-type ATMs (Fig. 2*A*). Also, we confirmed that the expression of extracellular matrix components, laminin C1, collagen 1a2, collagen 4a1, and collagen 4a2, increased at 5 weeks but decreased at 16 weeks, following the biphasic pattern described previously (Fig. 2*B*). In agreement with the switch from M2 to M1 profiles, genes encoding the M1 markers MCP1, interferon-β, TNF-α,

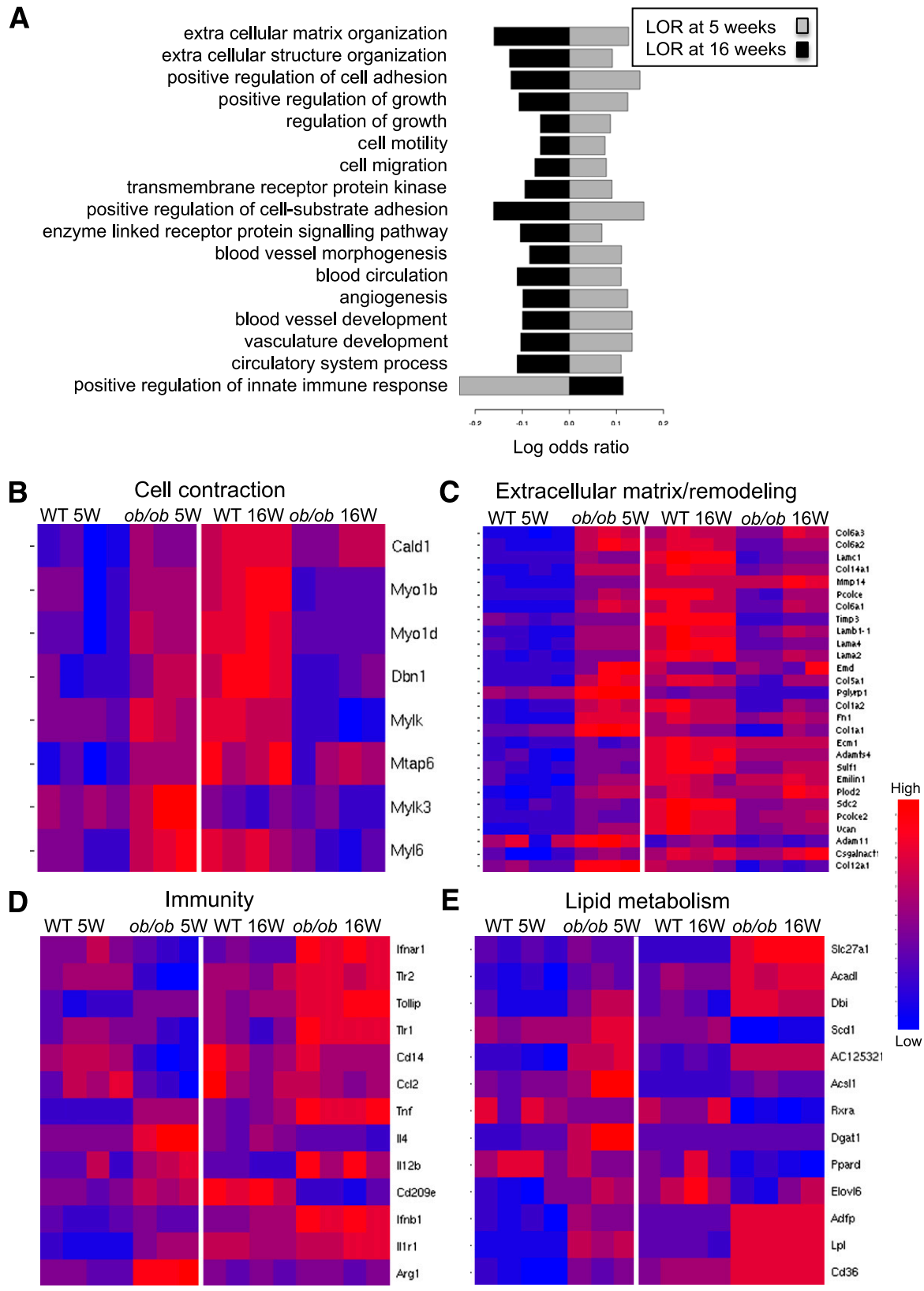

FIG. 1. Affymetrix microarray profiling of ATMs. Transcriptomic analysis of total RNA from wild-type (WT) versus *ob/ob* ATMs was done using mouse gene ST1.0 Affymetrix array. *A*: GO pathway analysis revealed a biphasic regulation of several biological pathways upregulated. For each functional class, the LOR of overrepresentation in *ob/ob* compared with wild-type mice is presented. Gray bars represent LOR at 5 weeks and black bars at 16 weeks. Positive LOR implies overrepresentation of the functional class in *ob/ob* compared with wild-type mice, whereas negative LOR implies underrepresentation of the functional class in *ob/ob*. All terms presented were found to be significant at corrected $P < 0.05$ (see RESEARCH DESIGN AND METHODS). *B–E*: The heat maps show selected groups of genes, sorted by biological function, differentially expressed when comparing wild-type to *ob/ob* mice at 5 or 16 weeks. The red color represents high-normalized expression levels and the blue color represents low expression levels. See the Supplementary Files for the complete list of genes.

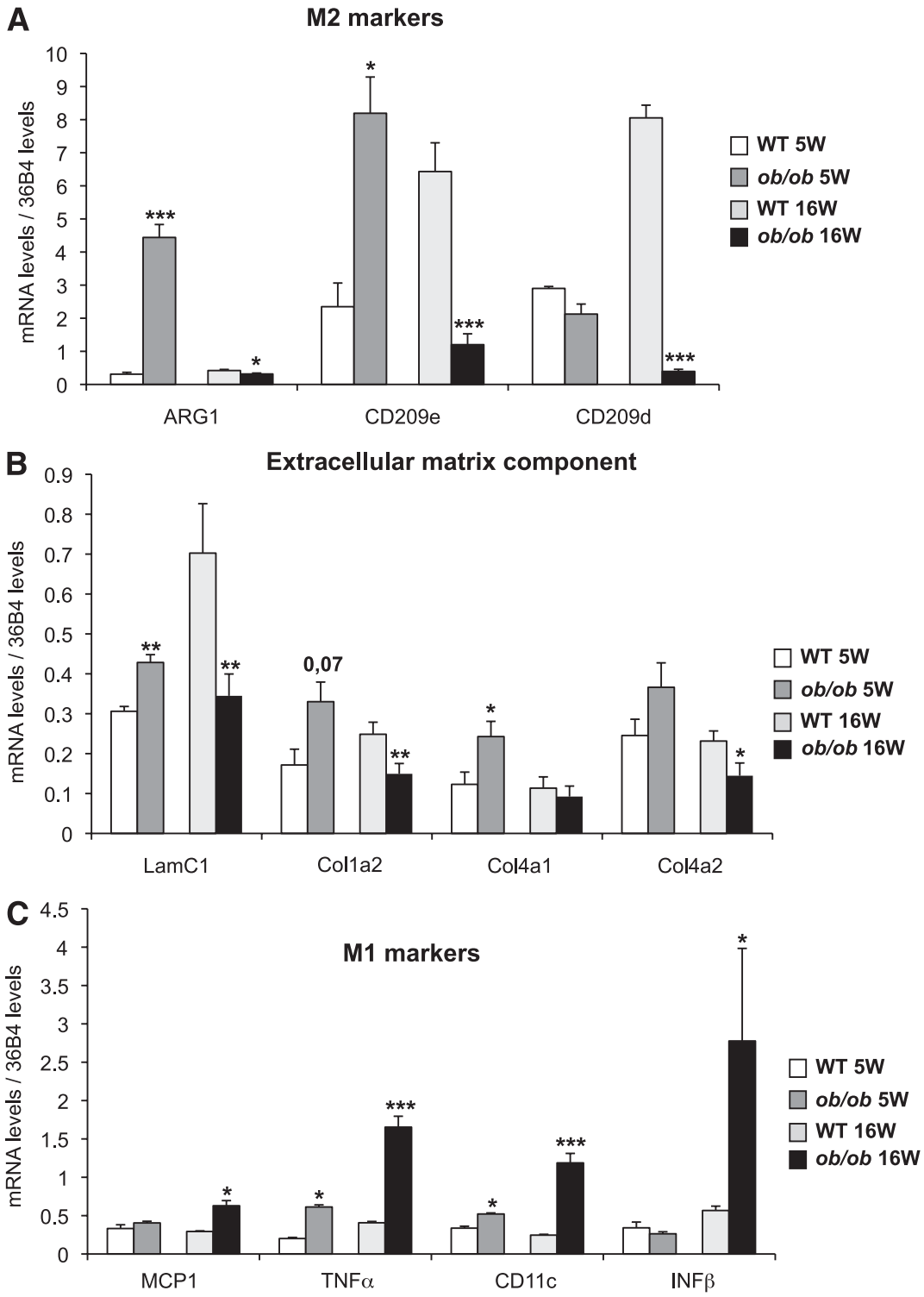

FIG. 2. Polarization profile of ATMs from *ob/ob* mice at 5 and 16 weeks. ATMs are isolated from perigonadal adipose tissue. The expression of anti-inflammatory (M2) markers (*A*), the extracellular matrix component (*B*), and proinflammatory (M1) markers (*C*) were evaluated by quantitative PCR using the standard curve method. The expression levels were normalized by the amount of 36B4. The bars represent the SEs and significant differences were as follows: **P* < 0.05; ***P* < 0.005; ****P* < 0.001. Males, *n* = 20 per group for 5-week-old mice and *n* = 16 per group for 16-week-old mice (see RESEARCH DESIGN AND METHODS).

and CD11c were markedly induced at 16 weeks of age in *ob/ob* mice in ATMs (Fig. 2*C*). Together, these transcriptional data indicate that in early stages of positive energy balance, ATMs have a predominantly anti-inflammatory M2 profile and that severe obesity and insulin resistance cause downregulation of M2-associated genes and induction of the M1 proinflammatory gene repertoire.

We confirmed these results in a diet induced obesity (DIO) model. In this model, we also observed a biphasic gene-expression profile in which *ARG1* was initially induced

after 1 month of the HFD (Supplementary Fig. 4); however, after 6 months of the HFD, the development of obesity and insulin resistance was accompanied by decreased *CD209d* (M2) and increased *CD11c* (M1) mRNA levels.

Obesity is associated with the presence of foam-like ATMs. Because our ATM profiling experiments revealed an increase of mRNA levels of genes involved in lipid uptake and storage, we hypothesized that ATMs may accumulate lipids in severe obesity. Confocal images of ATMs from 16-week-old *ob/ob* mice revealed strong lipid accumulation compared with wild-type controls (Fig. 3*A*); this was already visible in ATMs from 5-week-old *ob/ob* mice, albeit of a smaller magnitude (Supplementary Fig. 5). As illustrated in Fig. 3*B*, F4/80$^+$ cells from 16-week-old *ob/ob* ATMs contained lipid droplets in their cytoplasm and morphologically resembled proatherosclerotic foam cells.

We performed flow cytometry analysis to further characterize the CD11b-positive cell-sorted fraction and determined the percentage of positive cells using a fixed threshold (see RESEARCH DESIGN AND METHODS). A total of 45% of the ATMs from 16-week-old *ob/ob* mice stained for bodipy and therefore were lipid loaded, whereas only 6% of ATMs from wild-type mice were bodipy positive (Fig. 3*C*). Parallel to this increase in lipids, the percentage of CD11c-positive cells in ATMs from obese mice was significantly higher (33 vs. 11%) compared with lean mice (Fig. 3*D*). In contrast, the number of cells staining for the M2 marker CD209a (which has a similar gene-expression profile to CD209d; data not shown) was lower in *ob/ob* mice (47%) compared with wild-type mice (82%) (Fig. 3*E*). Analysis of lipid content in ATMs with different polarized states showed that in obese mice, 34% of the ATMs were CD11c$^+$/Bodipy^{high} and 33% were CD209a$^+$/Bodipy^{high} (Fig. 3*F*). These two populations were residual in lean mice. In addition, flow cytometry revealed that one-third of the ATMs in obese, but not in wild-type, mice were double positive for CD11c+/CD209a+ ATMs (Supplementary Fig. 6*B*). Analysis of the lipid content of the different ATM subtypes (CD11c+/CD209a−, CD11c+/CD209a+, CD11c−/CD209a−, and CD11c−/CD209a+) in the obese mice (Fig. 3*G*) showed that 57% of the CD11c+/CD209a+ and 20% of CD11c+/CD209a− ATMs were bodipy^{high}. In contrast, most of the CD11c−/CD209a+, which could be considered as classically M2-polarized ATMs, were not lipid loaded. Similar results were observed using another M2 marker, CD206 (data not shown). Altogether, our data show that in *ob/ob* mice, a large proportion of ATMs are lipid loaded and positive for CD11c (M1) and revealed the existence of a unique ATM subtype, CD11c +/CD209a+, that in a high proportion of cases is lipid loaded, whereas CD11c−/CD209a+ ATMs (M2) display low bodipy levels.

Obesity induces opposite transcriptional patterns for genes encoding key proteins in lipid metabolism pathways in adipocytes versus ATMs. To address the possibility of lipid repartition between adipocytes and ATMs, we analyzed, in parallel, the expression of genes associated with lipid metabolism in isolated adipocytes and ATMs from 5- and 16-week-old wild-type and *ob/ob* mice.

Gene-expression analysis in adipocytes showed that the expression of peroxisome proliferator–activated receptor (*PPAR*) *γ1* was reduced in adipocytes from 5-week-old *ob/ob* mice (Fig. 4*A*) and further decreased at 16 weeks. The expression of *PPARγ2* was unchanged at 5 weeks of age but downregulated by 70% in adipocytes from 16-week-old insulin-resistant *ob/ob* mice compared with wild-type adipocytes (Fig. 4*B*). Similarly, expression of *FATP1* (Fig. 4*C*) and of *LPL* were downregulated at 16 weeks of age (Fig. 4*E*). These results indicate progressive deterioration in the ability of adipocytes to metabolize and store lipids in parallel with the development of obesity and insulin resistance.

Expression analysis of the same lipid-related genes in ATMs showed that unlike adipocytes, expression of *FATP1* increased in *ob/ob* mice compared with wild-type controls (30% increase at 5 weeks and 300% increase at 16 weeks). Furthermore, at 16 weeks, expression of *CD36* increased by 50% (Fig. 4*D*) and that of *LPL* (Fig. 4*E*) increased sixfold in ATMs from *ob/ob* mice. The expression of the gene-encoding ADRP, a marker of lipid accumulation, increased threefold in *ob/ob* ATMs at 16 weeks compared with wild-type ATMs (Fig. 4*F*). Similar results were confirmed using the DIO model showing opposite changes in the expression of genes associated with lipid metabolism in ATMs and adipocytes during the development of obesity (Supplementary Fig. 7). This is compatible with a model in which the development of obesity and insulin resistance is associated with lipid partitioning away from adipocytes and into ATMs.

As expected in 16-week-old *ob/ob* insulin-resistant mice, the expression of genes involved in the lipogenic pathway (such as those encoding fatty acid synthase [FAS], stearyl coenzyme A desaturase 1 [SCD1], elongation of long chain fatty acids 6 [Elovl6], and diglyceride acyl transferase 1 [DGAT1]) decreased in adipocytes (Fig. 4*G*). In ATMs, Elovl6 and DGAT1 initially increased at 5 weeks of age in *ob/ob* ATMs compared with wild-type ATMs but then were repressed at 16 weeks (Fig. 4*H*). FAS and SCD1 were unchanged at 5 weeks but were repressed at 16 weeks. Together, these data indicate that at 16 weeks, *ob/ob* ATMs accumulate lipids mainly via activation of lipid uptake and transport pathways. Moreover, lipogenic pathways in these cells are inactive. These observations directed our research toward the type of lipids accumulated in these cells.

Lipid analyses reveal differences in chain length and saturation of triglycerides in ATM and adipocytes. Our confocal and gene-expression observations in the two models of obesity indicate that increased lipid accumulation and/or specific lipid species may contribute to M1 ATM polarization. We initially observed increased accumulation of triglycerides (16-fold increase) and total cholesterol (2-fold increase) in ATMs from 16-week-old *ob/ob* mice compared with wild-type mice (Fig. 5*A* and *B*). Using a lipidomics approach, we found a twofold increase in the two most abundant triglyceride species, triglyceride (52:2) and triglyceride (54:3), in *ob/ob* ATMs (Fig. 5*C*), both formed by relatively short-chain fatty acids. However, not all triglycerides increased; levels of triglyceride (54:6), which is formed by polyunsaturated triglycerides, decreased by 40% in *ob/ob* compared with wild-type ATMs. This indicates that ATMs from obese mice accumulate more triglycerides, but these are selectively enriched for saturated, short-chain fatty acids. Similar lipidomic analysis of *ob/ob* adipocytes (Supplementary Fig. 9*C*) confirmed an increase in the most abundant triglyceride species in comparison with wild-type adipocytes. However, unlike ATMs, the increase in triglycerides in adipocytes was relatively enriched in triglycerides containing long-chain polyunsaturated fatty acids, such as triglyceride (56:7) and triglyceride (58:8) (Supplementary Fig. 10).

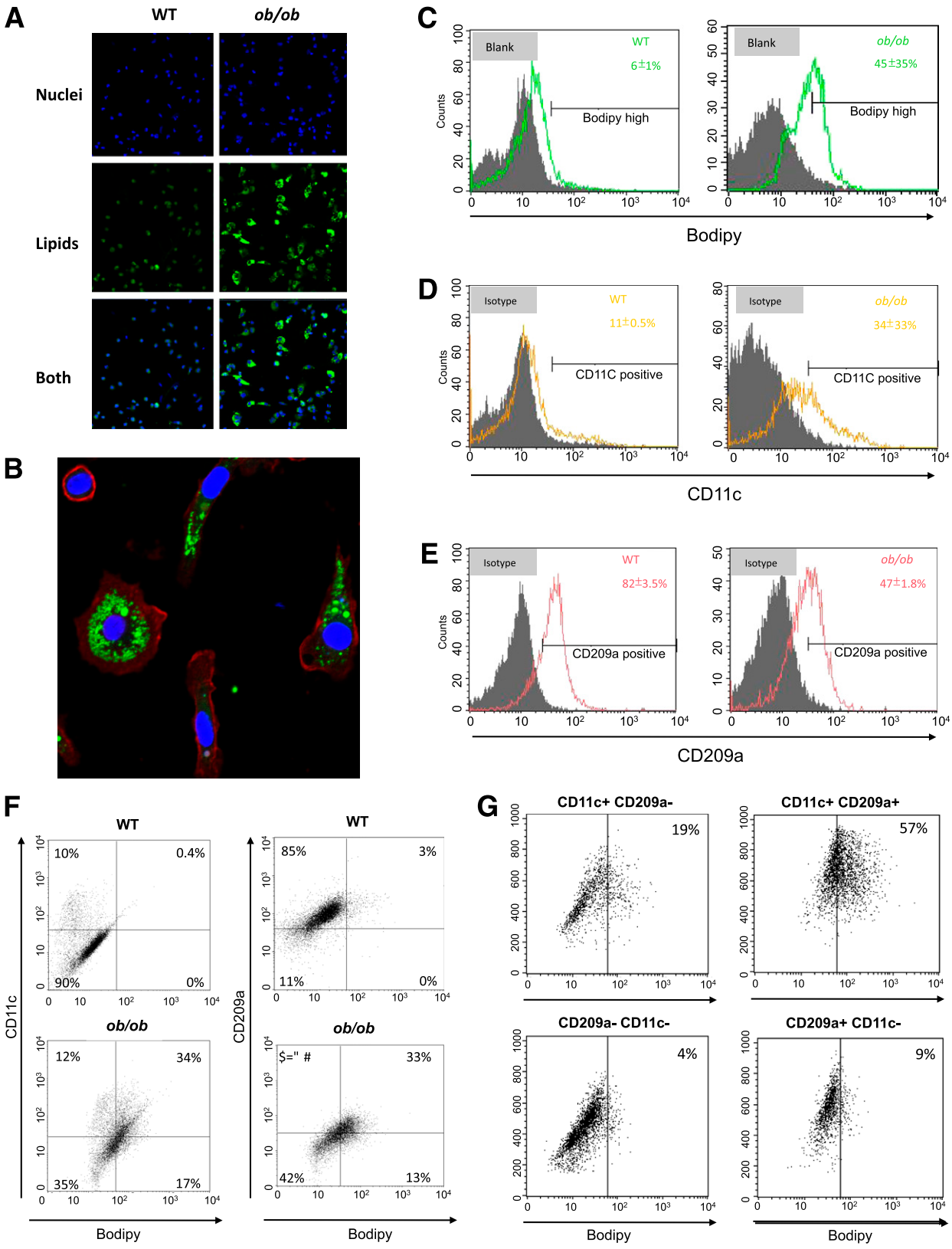

FIG. 3. Analysis of lipid content and polarization state of ATMs isolated from perigonadal adipose tissue from 16-week-old wild-type (WT) and *ob/ob* mice. *A*: Representative images of ATMs taken with a confocal microscope. Bodipy (green) detects neutral lipids and DAPI (blue) dyes nucleus. Images used ×10 magnification. *B*: ATMs from *ob/ob* mice with a ×40 magnification using bodipy, DAPI, and F4/80 staining (red). *C–E*: Flow cytometry quantification of lipid accumulation, CD11c+ ATMs, and CD209a+ ATMs. Filled and unfilled histograms represent ATMs stained with isotype control or fluorescent dye/antibodies, respectively. Panels show means ± SE of three independent experiments with similar results. *F*: Dot-plot images representing double staining (CD11c and bodipy, CD209a and bodipy) of ATMs. Images of corresponding isotype controls are shown in Supplementary Fig. 6. *G*: Flow cytometry quantification of bodipy content in different ATM subtypes from *ob/ob* mice. Representative data are from three independent experiments with similar results. (A high-quality digital representation of this figure is available in the online issue.)

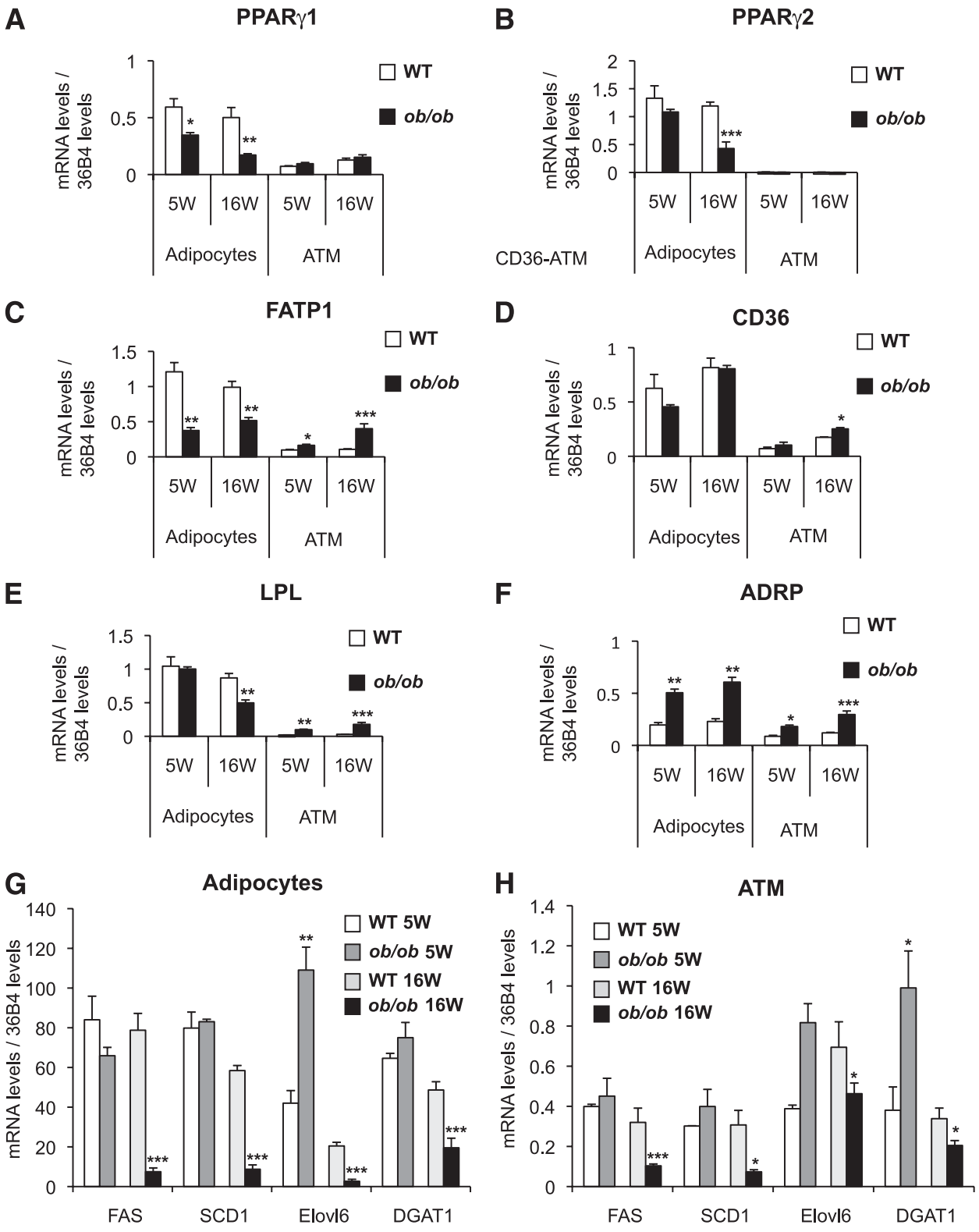

FIG. 4. Change in expression levels of the lipid metabolism gene in ATMs and adipocytes. *A–F*: The expression profile of key genes of the lipid metabolism were analyzed in parallel in ATMs and adipocytes. The mRNA levels of genes key in the lipogenesis pathway have been quantified in ATMs (*G*) and adipocytes (*H*). The expression levels were normalized by the amount of 36B4. The bars represent the SEs and significant differences were as follows: *$P < 0.05$; **$P < 0.005$; ***$P < 0.001$. Males, $n = 16$ per group (see RESEARCH DESIGN AND METHODS).

Our data also showed a global decrease in total phospholipid levels in *ob/ob* compared with wild-type ATMs. The amount of the most abundant plasmalogen phospholipid in macrophages, PE (38:4e), was lower in *ob/ob* ATMs than wild-type ATMs (Fig. 5*F*), a trend that was also observed with several other phosphatidylethanolamines (PEs), phosphatidylcholines (PCs), and sphingomyelins (SMs) (Fig. 5*D*, *E*, and *G*). Moreover, lipidomic analysis showed

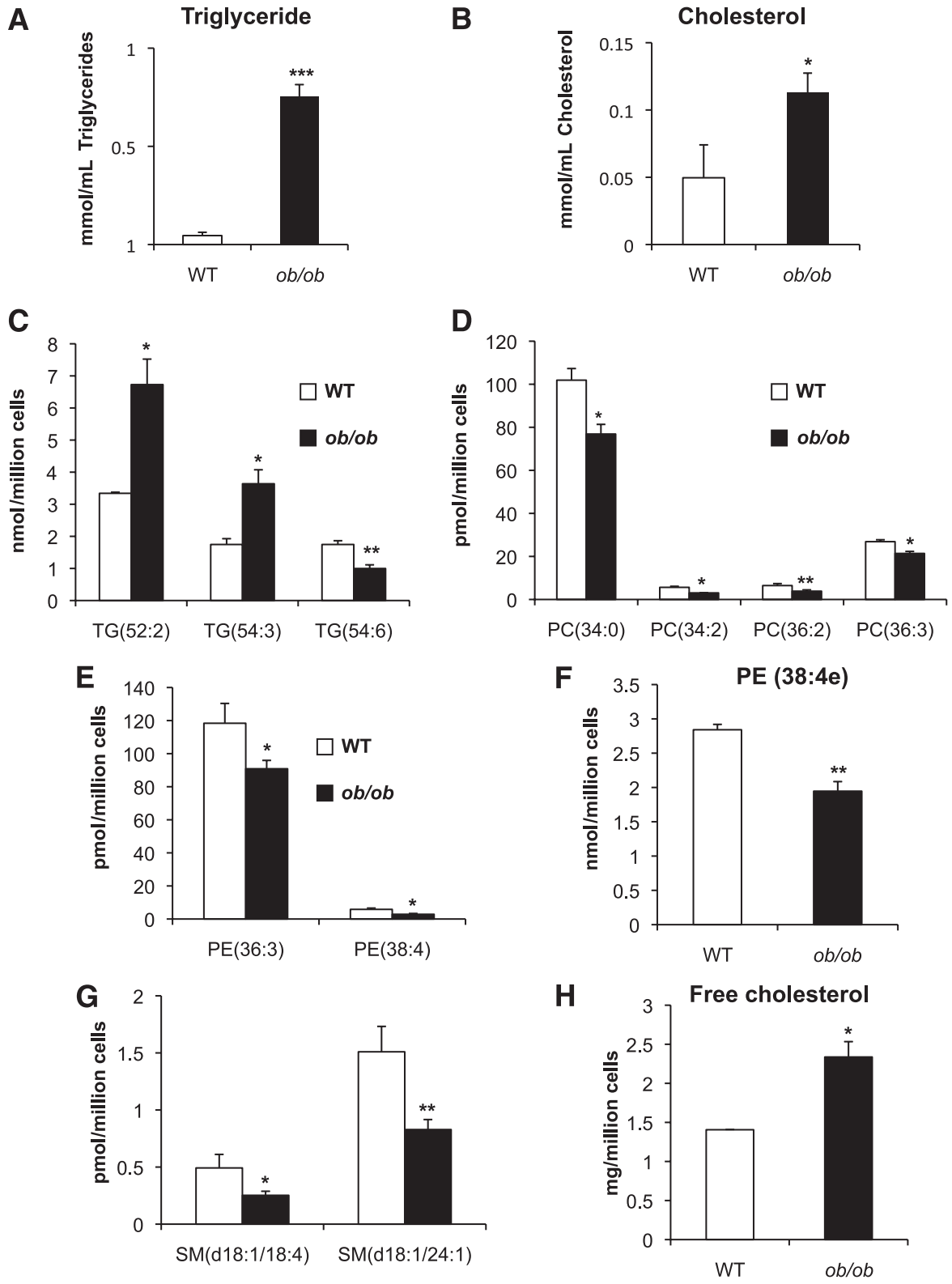

FIG. 5. Lipidomics profile of ATMs from 16-week-old *ob/ob* and wild-type (WT) mice. Absolute lipid concentrations of triglycerides (*A*) and cholesterol (*B*) assessed by colorimetric method and global lipid analysis showing significantly altered triglycerides (*C*), phosphotidylcholines (*D*), plasmalogen (*E*), phosphatidylethanolamine (*F*), sphingomyelin (*G*), and free cholesterol (*H*). The bars represent the SE of means and significant differences were as follows: *$P < 0.05$; **$P < 0.005$; ***$P < 0.001$. Males, $n = 16$ per group (see RESEARCH DESIGN AND METHODS).

a twofold increase of free cholesterol in ATMs from 16-week-old *ob/ob* compared with wild-type mice (Fig. 5*H*). Globally considered, lipidomic analyses of ATMs showed an increase in potentially cytotoxic lipid species (free cholesterol, short-chain, and more saturated triglycerides) and a depletion of protective lipids (long-chain and polyunsaturated triglycerides and plasmalogens) in *ob/ob* compared with wild-type ATMs. These changes occurred

simultaneously with the switch in ATM polarization from M2 to M1.

Impact of fatty acid length and saturation on macrophage polarization state. To support the hypothesis that the nature of the lipids stored might impact ATM polarization, we treated bone-marrow differentiated macrophages (BMDMs) with palmitate (C16), palmitoleate (C16:1), and with endolipide, a lipidic emulsion rich in polyunsaturated fatty acids. Our data (Fig. 6*A*) revealed that although palmitate treatment reduces *ARG1* (M2) expression levels, the mixture of polyunsaturated fatty acids strongly induced its expression compared with the control. In contrast, the expression of *TNF*α (M1 marker) was induced by palmitate, whereas palmitoleate and endolipide treatment reduced *TNF*α and *MCP1* (M1 markers) expression. The expression of *ADRP* was similarly induced in all three treatments, suggesting comparable lipid accumulation. Finally, only unsaturated lipids induced expression of PPARγ1 and its target gene *FATP1* (Fig. 6*B*). These results indicate that acute lipid loading with short, saturated fatty acids promotes M1 polarization, whereas ARG1 (M2) expression is induced by longer, more unsaturated fatty acids.

Thiazolidinedione treatment promotes and extends M2 polarization of ATM. We investigated whether improving the capacity of adipocytes to store lipid may affect the process of polarization (24). Therefore, we treated 4-week-old *ob/ob* mice with a standard diet containing 10 ppm rosiglitazone (thiazolidinedione [TZD]) for 12 weeks to assess TZD's effect on macrophage polarization and lipid partitioning. We confirmed that TZD treatment improved insulin sensitivity (Supplementary Fig. 8). At the same time, analysis of gene expression in ATMs revealed that expression of the M2 anti-inflammatory markers *ARG1*, *CD209d*, and *CD209e* markedly increased in ATMs from the TZD-treated group compared with control *ob/ob* mice (Fig. 7*A*). TZD treatment also reduced expression of *CD11c*, a marker of proinflammatory ATMs, by 50% (Fig. 7*B*).

Reciprocal effects of TZD treatment on lipid metabolic networks in adipocytes and ATMs. Gene expression of the PPARγ targets *ADRP*, *FATP1*, and *LPL* decreased in ATMs from *ob/ob* mice treated with rosiglitazone (Fig. 7*C*). Conversely, TZD treatment upregulated expression of *LPL*, *FATP1*, and *CD36* in adipocytes from the rosiglitazone-treated group (Fig. 7*D*). Although expression of *PPARγ1* in ATMs was unaltered by rosiglitazone treatment, expression of both *PPARγ1* and the more proadipogenic isoform, *PPARγ2*, increased in adipocytes, in agreement with the TZD-mediated increase in adipogenesis and lipid storage capacity (Fig. 7*D*).

Parallel lipidomic analysis revealed a marked decrease in ATM triglyceride levels from mice treated with

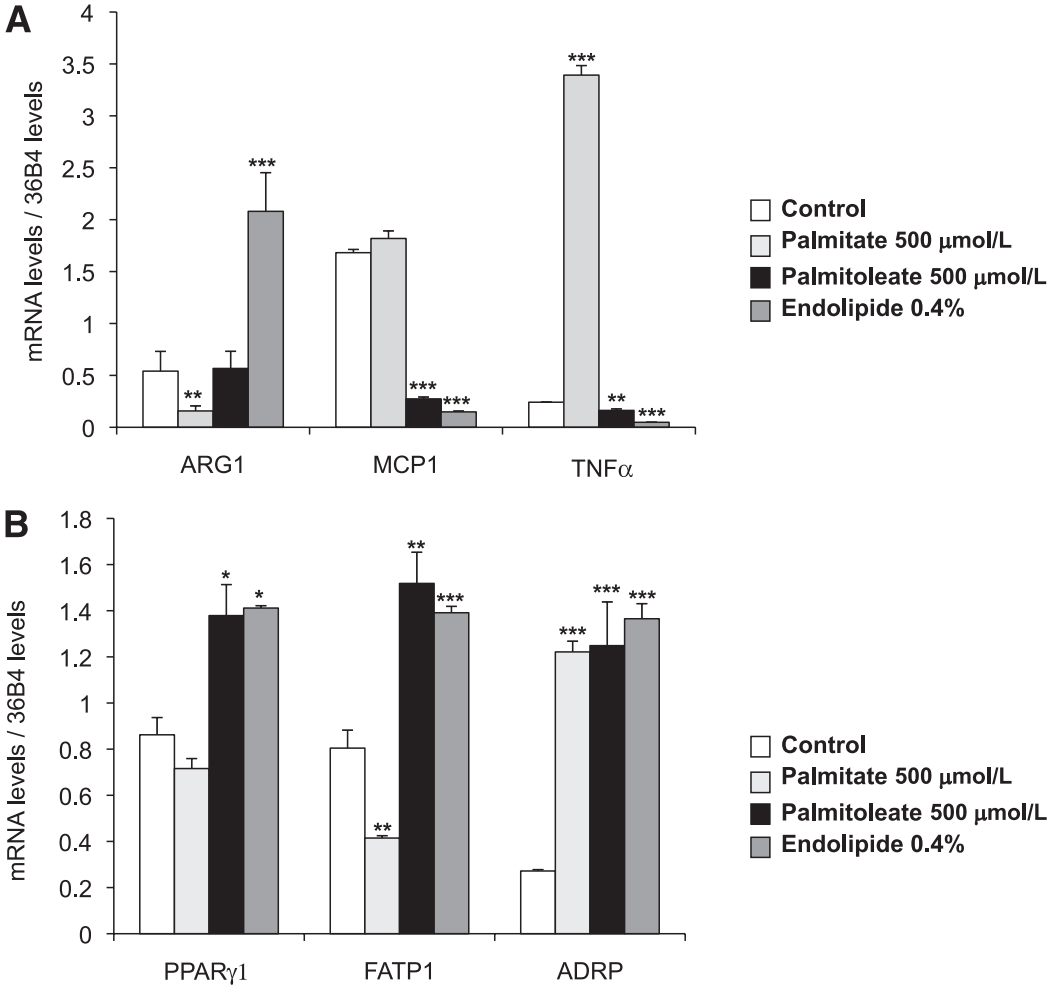

FIG. 6. BMDM treated with different types of fatty acids. BMDM are treated for 18 h with palmitate (500 μmol/L), palmitoleate (500 μmol/L), and endolipide (0.4%). *A*: The expression of M2/M1 markers and of key genes of the lipid metabolism were evaluated by quantitative PCR using the standard curve method. The expression levels were normalized by the amount of 36B4. The bars represent the SEs and significant differences were as follows: *$P < 0.05$; **$P < 0.005$; ***$P < 0.001$. Each condition has been done in triplicate ($n = 2$).

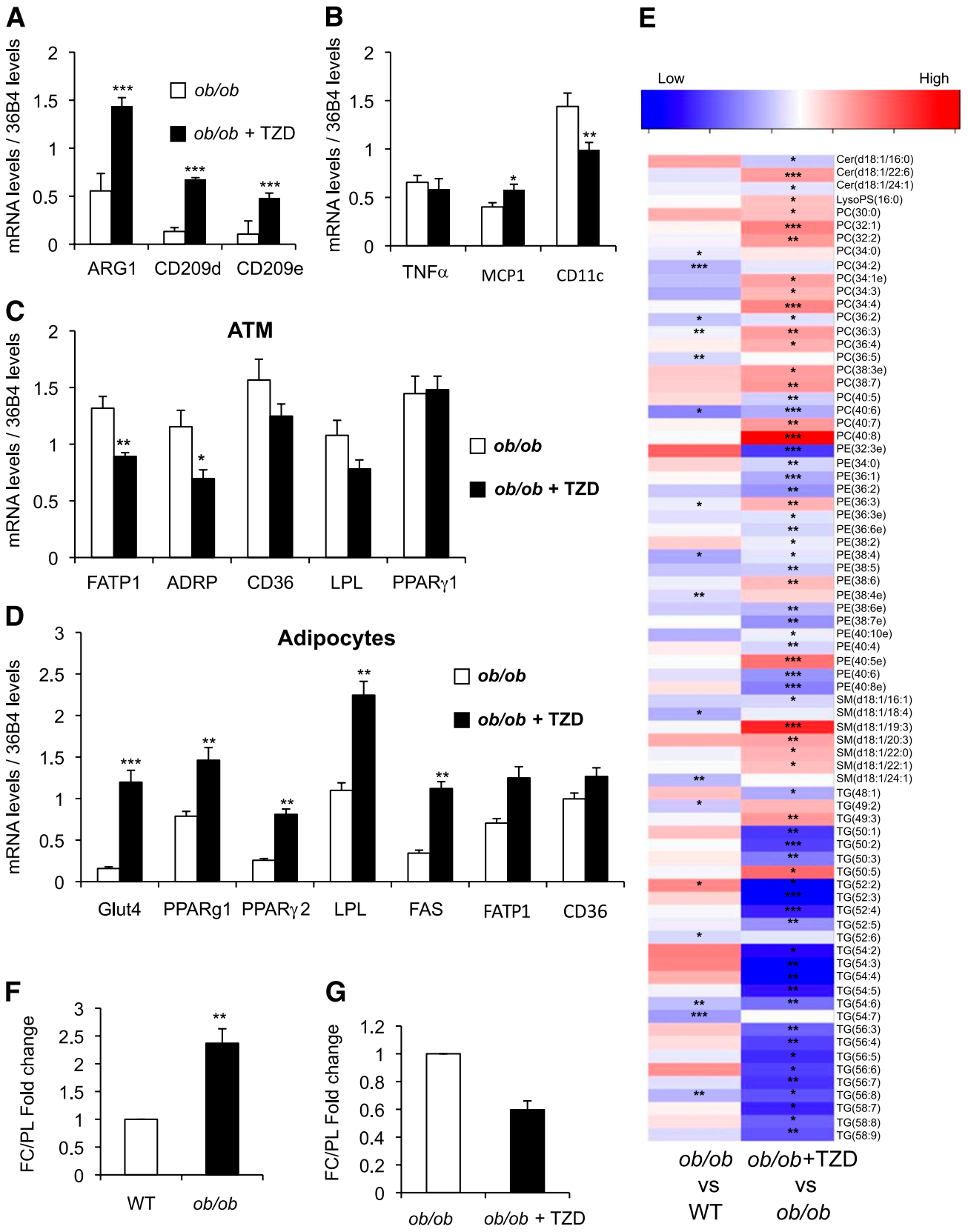

FIG. 7. Gene-expression and lipidomic profile of ATMs from *ob/ob* mice treated with rosiglitazone. Four-week-old male *ob/ob* mice (n = 7 in each group) were fed a standard diet with (*ob/ob* + TZD) or without (*ob/ob*) 10 ppm rosiglitazone for 12 weeks. ATMs were isolated from perigonadal adipose tissue at the end of the experiment. The expression levels of M2 markers (*A*), M1 markers (*B*), and key genes in lipid metabolism (*C*) were evaluated by quantitative PCR. *D*: Simultaneously, expression of genes involved in different metabolic pathways was measured in the adipocyte fraction. *E*: Fold change (log2) values of all the significantly altered lipids in ATMs are represented as a heat map. The ratio of free cholesterol to total phospholipid content (FC/PL) in (*F*) *ob/ob* vs. wild-type (WT) and (*G*) *ob/ob* vs. *ob/ob* TZD treated (*ob/ob*, n = 6; wild type, n = 3; control *ob/ob*, n = 9; TZD treated *ob/ob*, n = 10). The bars represent the SEs and significant differences were as follows: *$P < 0.05$; **$P < 0.005$; ***$P < 0.001$.

rosiglitazone (Fig. 7*E*). A comparison of lipid profiles induced by obesity in ATMs of wild-type versus *ob/ob* mice and the lipid profile observed in the obese model treated with rosiglitazone revealed reciprocal effects. Specifically, treating obese *ob/ob* mice with TZD decreased the two triglycerides, triglyceride (52:2) and triglyceride (54:3), which increased in ATMs from *ob/ob* mice compared with wild-type mice (Supplementary Fig. 9*C* and *D*). TZD treatment also increased concentrations of PC (36:3) and PE (36:3), the membrane phospholipids previously shown to decrease in ATMs from obese *ob/ob* mice. Furthermore, the ratio of free cholesterol to the total phospholipid content, an established correlate of cholesterol-induced cytotoxicity in atherosclerotic foam cells, also showed reciprocal effects (i.e., decreased in ATMs from TZD-treated mice compared with control animals) (Fig. 7*F* and *G*).

DISCUSSION

Obesity is associated with subclinical inflammation in adipose tissue. However, it remains unclear why the expansion of adipose tissue in obese individuals could attract macrophages to this tissue and trigger their proinflammatory response. In this article, we provide evidence that ATMs from obese, insulin-resistant murine models have quantitative/qualitative changes in lipid composition, which is associated with ATM polarization and the development of low-grade inflammation. Using one genetic and one diet-induced murine model of obesity, we obtained evidence to support changes in lipid-mediated cross-talk between adipocytes and ATMs during the progressive development of obesity and insulin resistance. The initial phase of this process is characterized by the induction of M2 anti-nflammatory markers in ATMs and is observed in the early stages of positive energy balance, when the adipose tissue is actively expanding and glycemia is relatively preserved. The M2 state is characterized by induction of genes involved in tissue remodeling/wound healing (25). This timing indicates that the M2 ATM phase may be a physiological adaptation to excess nutrient availability and adipose tissue expansion and remodeling.

The later phase is characterized by M1 ATM polarization and is associated with severe obesity and insulin resistance. Additional analysis of the metabolic changes taking place simultaneously in adipocytes and ATMs lend support to a model in which lipid-induced toxicity is an important determinant of the proinflammatory switch in ATM polarization. Indeed, our results reveal that nearly 50% of the ATMs from obese mice accumulate lipids and resemble proatherosclerotic foam cells. Lipid accumulation was associated with increased CD11c+ ATMs (M1) and decreased CD209a+ ATMs (M2). However we identified a unique subclass of ATMs that were positive for both CD209a+ and CD11c+ and that were in large proportion lipid loaded. This result suggests that increased lipid load may contribute to the transition from M2 to M1 associated with obesity-induced insulin resistance.

Parallel analyses of ATMs and adipocytes revealed opposite effects on gene expression and lipid composition of the two cell types. The lipid gene networks that were upregulated in ATMs were downregulated in adipocytes. In terms of lipids under positive energy balance, ATMs accumulate free cholesterol and short-chain, saturated triglycerides and are depleted of antioxidant plasmalogen phospholipids. The change in length and saturation of fatty acids might be partially explained by the decrease in mRNA encoding SCD1 and Elovl6 at 16 weeks of age in *ob/ob* mice ATMs. We also observed reciprocal changes in the lipidome of adipocytes from obese mice compared with lean control mice characterized by the depletion of saturated triglyceride species that appear to be accumulated in ATMs. These results reveal a degree of selectivity with respect to the ATM polarization–dependent partitioning of lipids between adipocytes and macrophages. Furthermore, our findings support the concept of lipid species–specific pathogenic mechanisms promoting M1 ATM polarization and suggest the possibility of preventing this by nutritional manipulation of fatty acids. The effects of treatment of BMDM with different fatty acid species demonstrate that long, saturated fatty acids induced *ARG1* (M2) expression and repressed the expression of M1 markers, whereas treatment with palmitate (saturated fatty acids) induced *TNFα* gene expression. Through these results, we speculate that the decrease in the expression of SCD1 and Elovl6 noted earlier may have a direct effect on ATM polarization.

From our model, we hypothesize that increasing the capacity of adipocytes to store lipid should either prevent or retard the switch in ATM polarization. We used rosiglitazone to promote fat deposition in adipocytes. Our results reveal that treatment with rosiglitazone increases the expression of prolipogenic genes in adipocytes, in association with the improvement in insulin sensitivity. Conversely, simultaneous analysis of lipid-gene networks in ATMs revealed decreased expression of FATPs and of *ADRP*. However, although both adipocytes and macrophages express PPARγ (26), TZD treatment only modulated PPARγ and its target gene expression in adipocytes. Thus, adipocytes appear to be the main target for PPARγ-dependent effects of rosiglitazone in our murine models. Our results indicate that rosiglitazone facilitates fat deposition in adipocytes, sequestering it away from ATMs. In support of this, recent evidence (27) shows that selective activation of PPARγ in adipocytes, but not in macrophages, is sufficient for whole-body insulin sensitization equivalent to systemic TZD treatment. This adipocentric model of the TZD effect is supported by our lipidomic analysis, which confirms the decrease in lipid accumulation in rosiglitazone-treated ATMs. The finding that TZD decreases triglyceride and free cholesterol levels in macrophages supports the link between lipid accumulation in these cells and the switch to the proinflammatory M1 polarization state.

Our data indicate that the initial lipid-induced M2 polarization might contribute to physiological remodeling of adipose tissue. Interestingly, Scherer et al. (28) have shown that several collagen isoforms are upregulated in adipose tissue from *ob/ob* mice and that deletion of collagen 6 in an *ob/ob* background improves insulin sensitivity and decreases adipose tissue inflammation despite marked increases in adipocyte size. Altogether, these findings raise the question of the importance of ATM-mediated remodeling in the context of adipose tissue expansion.

Finally, we observed an increase in free cholesterol levels and FC:PL and a decrease in several phospholipid species in lipid-loaded ATMs. Together, these alterations in lipid content may trigger a lipotoxic cascade, as previously described for induction of the inflammatory pathways and endoplasmic reticulum stress (29). Recent findings demonstrate the role of lipid-induced endoplasmic reticulum stress in arterial-wall macrophages (30); it will be interesting to investigate whether activation of this same pathway in

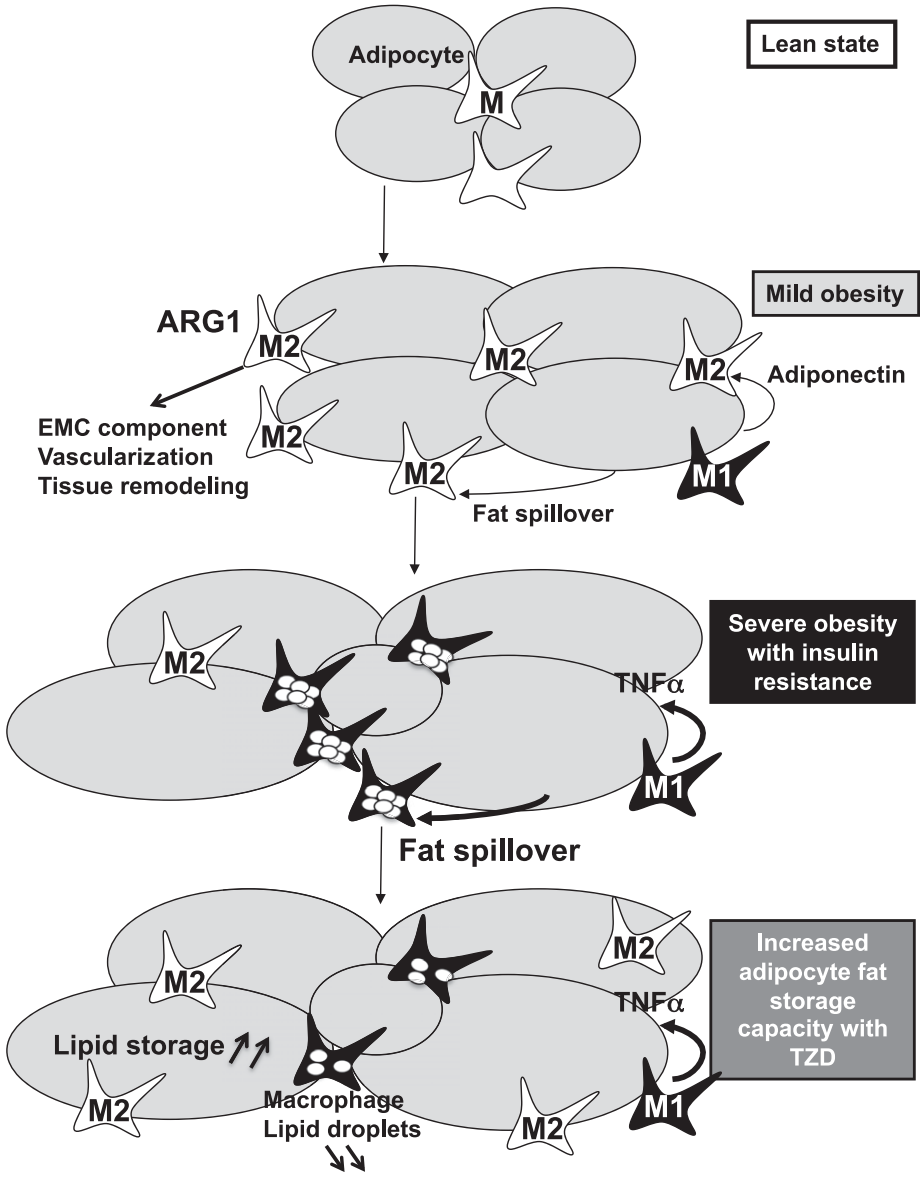

FIG. 8. Model of macrophage polarization and foam-cell formation in obese adipose tissue. The initial phase of this process was characterized by the induction of M2 anti-inflammatory markers and gene-expression pathways related to extracellular components. The second phase of this process, typically associated with severe obesity and insulin resistance, was characterized by M1 polarization of ATMs and was characterized by lipid-loaded ATMs resembling proatherosclerotic foam cells. Rosiglitazone treatment prevents lipid accumulation in ATMs and maintains their M2 profile by promoting adipocyte differentiation and fat deposition in adipocytes.

ATMs has a role in the development of insulin resistance–induced obesity.

In brief, in this article we focused on the early pathogenic events triggering the ATM polarization switch observed in obesity. We reveal this to be a biphasic process: the initial M2 profile is associated with positive energy balance and expansion of adipose tissue and is followed by a proinflammatory M1 profile in a context of maximal adipose tissue expansion, insulin resistance, and metabolic disturbance. This polarization switch is accompanied by progressive lipid accumulation in ATMs, leading to the formation of foam-like cells in adipose tissue. These observations can be integrated in a pathogenic model that includes the concept of exhausted adipose tissue expandability and adipocyte dysfunction that leads to lipid leakage and repartitioning of lipids away from adipocytes into ATMs. Cell-specific, reciprocal regulation of gene and biochemical networks associated with lipid metabolism in adipocytes and ATMs facilitate this process (Fig. 8). Based on this model, and supported by our rosiglitazone experiments, we propose that pharmacological/nutritional interventions that either improve adipocyte function or prevent lipid-induced ATM toxicity may provide novel therapeutic strategies to uncouple obesity from its metabolic complications.

ACKNOWLEDGMENTS

This study was supported by a Wellcome Trust Programme grant to A.V.-P. and S.O., FP7 Hepadip grants to A.V.-P. and M.O., MRC CORD, MRC programme and BHF grants to A.V.-P. and by grants from the Spanish Ministry of Science and Innovation (SAF2009-07466) and "Marató TV3" to M.R. The CNIC is supported by the Spanish Ministry of Science and Innovation and the Pro-CNIC Foundation. This work

is also supported by Grant BIO BIO2008-04212 from the Spanish Ministry of Science and Innovation to J.D. N.B. is funded by "fundacion IMABIS."

No potential conflicts of interest relevant to this article were reported.

X.P. researched data, designed the experiments and wrote the manuscript. C.Y.L.M. and V.R.V. researched data and analyzed data. V.N. and L.F. researched data. D.M. researched data and performed computer analysis. K.I., A.C., and N.B. researched data. S.O. contributed to scientific discussion and scientific review of the manuscript. J.K.S. contributed to scientific discussion and experimental design. J.D. contributed to scientific discussion and analyzed data. M.O. contributed to scientific discussion and data analysis. M.R. contributed to experimental design and wrote the manuscript. A.V.-P. designed the study and wrote the manuscript.

REFERENCES

1. Hotamisligil GS. Inflammation and metabolic disorders. Nature 2006;444:860–867
2. Cawthorn WP, Sethi JK. TNF-alpha and adipocyte biology. FEBS Lett 2008;582:117–131
3. Weisberg SP, McCann D, Desai M, Rosenbaum M, Leibel RL, Ferrante AW Jr. Obesity is associated with macrophage accumulation in adipose tissue. J Clin Invest 2003;112:1796–1808
4. Lumeng CN, Deyoung SM, Bodzin JL, Saltiel AR. Increased inflammatory properties of adipose tissue macrophages recruited during diet-induced obesity. Diabetes 2007;56:16–23
5. Lumeng CN, Bodzin JL, Saltiel AR. Obesity induces a phenotypic switch in adipose tissue macrophage polarization. J Clin Invest 2007;117:175–184
6. Lumeng CN, DelProposto JB, Westcott DJ, Saltiel AR. Phenotypic switching of adipose tissue macrophages with obesity is generated by spatiotemporal differences in macrophage subtypes. Diabetes 2008;57:3239–3246
7. Patsouris D, Li PP, Thapar D, Chapman J, Olefsky JM, Neels JG. Ablation of CD11c-positive cells normalizes insulin sensitivity in obese insulin resistant animals. Cell Metab 2008;8:301–309
8. Virtue S, Vidal-Puig A. It's not how fat you are, it's what you do with it that counts. PLoS Biol 2008;6:e237
9. Virtue S, Puig AV. Adipose tissue expandability, lipotoxicity and the metabolic syndrome—an allostatic perspective. Biochim Biophys Acta 2010;1801:338–349
10. Sethi JK, Vidal-Puig AJ. Thematic review series: adipocyte biology. Adipose tissue function and plasticity orchestrate nutritional adaptation. J Lipid Res 2007;48:1253–1262
11. Vidal-Puig A, Unger RH. Special issue on lipotoxicity. Biochim Biophys Acta 2010;1801:207–208
12. Virtue S, Vidal-Puig A. Adipose tissue expandability, lipotoxicity and the metabolic syndrome: an allostatic perspective. Biochim Biophys Acta 2010;1801:338–349
13. Prieur X, Roszer T, Ricote M. Lipotoxicity in macrophages: evidence from diseases associated with the metabolic syndrome. Biochim Biophys Acta 2009;1801:327–337
14. Tan CY, Vidal-Puig A. Adipose tissue expandability: the metabolic problems of obesity may arise from the inability to become more obese. Biochem Soc Trans 2008;36:935–940
15. Affymetrix power tools [article online]. Available from http://www.affymetrix.com/partners_programs/programs/developer/tools/powertools.affx. Accessed 15 September 2009, copyright 2009
16. Irizarry RA, Hobbs B, Collin F, et al. Exploration, normalization, and summaries of high density oligonucleotide array probe level data. Biostatistics 2003;4:249–264
17. Bolstad BM, Irizarry RA, Astrand M, Speed TP. A comparison of normalization methods for high density oligonucleotide array data based on variance and bias. Bioinformatics 2003;19:185–193
18. Smyth GK. Linear models and empirical bayes methods for assessing differential expression in microarray experiments. Stat Appl Genet Mol Biol 2004;3:e3
19. Sartor MA, Leikauf GD, Medvedovic M. LRpath: a logistic regression approach for identifying enriched biological groups in gene expression data. Bioinformatics 2009;25:211–217
20. Montaner DDJ, Dopazo J. Multidimensional gene set analysis of genomic data. PLoS ONE 2010;5:e10348
21. Medina ICJ, Carbonell J, Pulido L, et al. Babelomics: an integrative platform for the analysis of transcriptomics, proteomics and genomic data with advanced functional profiling. Nucleic Acids Res 2010;38(Suppl.):W210–W213
22. Medina-Gomez G, Yetukuri L, Velagapudi V, et al. Adaptation and failure of pancreatic beta cells in murine models with different degrees of metabolic syndrome. Dis Model Mech 2009;2:582–592
23. Kanehisa MAM, Araki M, Goto S, et al. KEGG for linking genomes to life and the environment. Nucleic Acids Res 2008;36(Database issue):D480–D484
24. Bouhlel MA, Derudas B, Rigamonti E, et al. PPARgamma activation primes human monocytes into alternative M2 macrophages with anti-inflammatory properties. Cell Metab 2007;6:137–143
25. Mills CD. Macrophage arginine metabolism to ornithine/urea or nitric oxide/citrulline: a life or death issue. Crit Rev Immunol 2001;21:399–425
26. Ricote M, Li AC, Willson TM, Kelly CJ, Glass CK. The peroxisome proliferator-activated receptor-gamma is a negative regulator of macrophage activation. Nature 1998;391:79–82
27. Sugii S, Olson P, Sears DD, et al. PPARgamma activation in adipocytes is sufficient for systemic insulin sensitization. Proc Natl Acad Sci USA 2009;106:22504–22509
28. Khan T, Muise ES, Iyengar P, et al. Metabolic dysregulation and adipose tissue fibrosis: role of collagen VI. Mol Cell Biol 2009;29:1575–1591
29. Devries-Seimon T, Li Y, Yao PM, et al. Cholesterol-induced macrophage apoptosis requires ER stress pathways and engagement of the type A scavenger receptor. J Cell Biol 2005;171:61–73
30. Erbay E, Babaev VR, Mayers JR, et al. Reducing endoplasmic reticulum stress through a macrophage lipid chaperone alleviates atherosclerosis. Nat Med 2009;15:1383–1391